

# Cancer Growth Treatment by Adaptive Robust Immune Pole Placement Controller with Different Structures

Mohammed Ayad Hussein, Ekhlas Hameed Karam

**Abstract**—Despite medical and technological advancements that can detect and cure many cancer forms, cancer incidence and mortality rates are rising worldwide. A tumor-killing virus that infects and analyzes cancer cells while leaving most normal cells intact is known as an oncolytic virus. The mathematical model of interact between tumor cells and oncolytic viruses used to provide closely look to these technics used in cancer treatment. In this article, an Adaptive Robust Immune Pole Placement (ARIPP) controller based on an Improved Crow Search Algorithm (ICSA) has been suggested to deliver oncolytic viruses. The control method was evaluated on a computer using MATLAB simulation. Furthermore, the dynamic uncertainty also tested, results show tumor cells reduced to a specific therapeutic zone. The suggested controller ARIPP I structure shows more excellent performance than structure II and III structure by 3.2707%, 3.5452%, respectively.

**Keywords**— Oncolytic virotherapy, feedback mechanism, robust control, ICSA, state feedback.

## I. INTRODUCTION

Cancer is one of the most prevalent illnesses globally, with over 17 million cases reported in 2018 and predictions that this number would rise to 23.6 million by 2030 [1],[2]. The term “cancer” refers to a group of illnesses with several features, including uncontrolled cell proliferation and spread into adjacent tissues [3]. Because of the disease’s complexity and heterogeneity, choosing the right drug, dosage, and treatment plan have become problematic. Therefore, cancer scientists and researchers all around the globe are working to make better use of the current therapeutic choices to enhance treatment results and patient quality of life [4]. Several treatment regimens used in cancer therapy, such as managing a low dosage for an extended period or a high dose followed by a low dose [4].

Virotherapy is a cancer treatment that uses viruses’ capacity to infect and multiply in cancer cells to kill them [5]. These viruses are known as oncolytic viruses. Adenovirus, Reovirus, Measles, Herpes Simplex, and Vesicular-Stomatitis Virus (VSV) are among the most effective viruses against malignant tumors [6].

Mathematical models aid in the prediction of cancer’s future behavior. These models may be used to enhance and optimize the effect of many variables such as viral genetics,

dose, and injection schedules. Unfortunately, performing such expectations in vivo, vitro, or clinical studies is difficult, hazardous, and costly [1].

Much research has been done to find a more systematic approach for tuning control parameters efficiently and make them more robust and powerful. The current trend is to utilize a natural-inspired metaheuristic algorithm to tackle complex problems and are found to be surprisingly very efficient [7].

Metaheuristic algorithms based on biological principles, swarm behavior, and chemical or physical processes are nature-inspired optimization algorithms. For example, the crow search algorithm (CSA), inspired by crow behavior, was first presented in [8], with its primary use in solving engineering problems with limitations.

Biological information processing systems are more adaptable than the technologies that are presently accessible. As a result, it is feasible to create a system that outperforms traditional methods [9]. The immune system is complicated made up of a variety of immune cells and communication pathways. Nevertheless, it is an excellent mechanism for protecting the human body from infections and external objects [10].

Much prior research has shown interactions between virotherapy and control theory. For example, Yongmei et al. in [11] utilized optimal control, virotherapy, and targeted control to decrease the tumor size. Nonetheless, since the model they employed lacked an equilibrium point, the tumor might strongly return.

To enhance the outcomes of chemotherapy and virotherapy, Joseph et al. in [12] utilize an optimal control for chemotherapy in conjunction with virotherapy. Consequently, the findings indicated that the treatment program was successful, and the quantity of optimum medicine for chemotherapeutic and viral combinations is half of the corresponding maximum tolerated dosages.

In [13], Anita et al. utilize the state-dependent algebraic Riccati equation (SDARE) (similar to linear LQR, but SDARE is a nonlinear method used with nonlinear control) to extract the optimum virotherapy infusion rate utilizing robust and optimal control. As a result, the number of cancer cells is decreased to 60%.

Anelone et al. in [14] design the impulsive controller to deliver a personalized dose for each case, and the feedback controller showed a tumor reduction potential better than that obtained by experimental protocols, but a long process of tuning by trial and error necessary to avoid saturation due to the calculation of negative values of the input controller.

In [15] Villa-Tamayo et al. using impulsive control theory, offer a nonlinear estimate and control method for determining viral injection dosages. The extended Kalman

Manuscript received September 9, 2021.

Mohammed Ayad Hussein, M.Sc. Student, Mustansiriyah University, College of Engineering, Computer Engineering Department, Palestine Street, 14022, Baghdad, Iraq (e-mail: mohammediyad95@gmail.com).

Dr. Ekhlas Hameed Karam, Assistant Prof., Mustansiriyah University, College of Engineering, Computer Engineering Department, Palestine Street, 14022, Baghdad, Iraq (e-mail: ek\_karam@yahoo.com).

filter and nonlinear model predictive control

Symbol	$S_0$	$I_0$	$V_0$	$r$	$K$	$\beta$	$d_I$	$d_V$	$\alpha$
$S_1$	238.3535	0	0	0.0378	8466.8	1.12	2	2.0872	2
$S_2$	200.0340	0	0	0.0733	3179.1	1.4987	1.9995	3.2287	2.0015
$S_3$	101.5400	0	0	0.0224	4922.4	0.2	2	3.5	2
$S_4$	140.3436	0	0	0.0316	8317.1	1.2108	0.1	1.8730	3.7748
$S_5$	128.1481	0	0	0.0603	936.4293	1.3606	0.1	1.8416	3.7541
unit	cells	cells	virus	day <sup>-1</sup>	cells $\times 10^6$	day <sup>-1</sup>	day <sup>-1</sup>	day <sup>-1</sup>	virus $\times 10^9$

(iNMPC+hEKF) were used to create the system controller. The control method demonstrates the need for a more robust strategy to deal with greater plant-model incompatibilities.

In this paper, the pole placement is used as a controller based on an improved Crow Search Algorithm (ICSA) for parameter optimization to track the number of viruses provided to patients. In addition, the body's immune mechanism is used here to enhance the performance of the pole placement controller.

The other parts of this paper are arranged as follows: in the second part, the mathematical model is described; in the third part, the immune system developed; in the fourth part, the ICSA is shown. The suggested adaptive robust immune pole placement structures controller is defined in the fifth section. In the sixth part, the simulation results and an evaluation of the proposed controllers are discussed, and the conclusion is given in the last section.

## II. MODEL OF INTERACTION BETWEEN ONCOLYTIC VIRUS AND CANCER CELLS

The oncolytic adenovirus ADPEGHER was utilized to treat solid tumors in nude mice in earlier experimental and mathematical studies [14], [16 -18]. Because these naked mice have no immune system, the tumor decrease is entirely attributable to the oncolytic virotherapy. The studies began with mice that had 90 to 300 cancer cells. Each experiment injects  $10^{10}$  virus particles according to a predetermined method on days 0, 2, and 4. According to work in [17], the interaction between oncolytic virus and cancer cells can mathematically be represented using ordinary differential equations [17]:

$$\begin{aligned} \dot{S}(t) &= r \log\left(\frac{K}{S(t)}\right) - \frac{\beta V(t)S(t)}{S(t) + I(t) + \epsilon} \\ \dot{I}(t) &= \frac{\beta V(t)S(t)}{S(t) + I(t) + \epsilon} - d_I I(t) \\ \dot{V}(t) &= U_v(t) - d_V V(t) + \alpha d_I I(t) \end{aligned} \quad (1)$$

where,  $S$  denotes the density of susceptible tumor cells ( $\times 10^6$  cells),  $t$  represents the time,  $r$  is the tumor growth (day<sup>-1</sup>),  $K$  describes the caring capacity (cell  $\times 10^6$ ),  $\beta$  is the tumor cells rate of infection (day<sup>-1</sup>),  $I$  refers to the density of infected tumor cells ( $\times 10^6$  cells),  $d_I$  is the infected tumor cells death rate (day<sup>-1</sup>),  $V$  is the density of virus particles ( $\times 10^9$  virus),  $d_V$  is the viral decay (day<sup>-1</sup>) and  $\alpha$  viral burst size (virus  $\times 10^9$ ). The characteristics of the interaction between oncolytic virens and the tumor cells model utilized in this study are shown in Table I.

**Table I:** Parameters and initial conditions values [17].

$T=S+I$  is the total number of tumor cells,  $\epsilon$  is a small value ( $\epsilon > 0$ ) set to avoid singularity occurring as  $(S+I)$  approaches zero.

The model's input expresses the injection of virus particles  $U_v(t)$ . While  $T$  represents the model's output. The tumor volume calculated as  $T = 0.523 \times H \times B^2$  where  $(H)$  is the height and  $(B)$  is the breadth. Both  $(H)$  and  $(B)$  were measured with a caliper [16]. Then, assuming a density of  $10^6$  cells per mm<sup>3</sup>,  $T$  is calculated [17].

## III. IMMUNE FEEDBACK MECHANISM

As a control system, the biological immune system has high robustness and self-adaptation capacity even in severe disruptions and unpredictable circumstances. It may develop subsequent antibodies to prevent invasion by a foreign antigen [19]. After mixing antigens and antibodies, a sequence of biological reactions may occur, and the antigen is eliminated using phagocytes or special enzymes. Antibodies and lymphocytes make up the immune response. The lymphocyte is made up of  $B$  cells from the bone marrow and  $T$  cells from the thymus.  $T$  cells are divided into helper  $T$  cells  $T_H$  and suppressor  $T$  cells  $T_S$  [19].

When a cell receives an antigen signal, it sends the information to  $T_H$  and  $T_S$ , stimulating  $B$  cells to develop antigen-resisting antibodies. Thus, all of the received simulations of  $B$  cells were obtained using the immune feedback control system.

$$T_H(t) = K_1 \lambda(t) \quad (2)$$

$$T_S(t) = K_2 \{f[\Delta B(t-d)]\} \lambda(t) \quad (3)$$

$$B(t) = T_H(t) - T_S(t) \quad (4)$$

$$\dot{B}(t) = K_1 \{1 - \eta_0 f[\Delta B(t-d)]\} \lambda(t) \quad (5)$$

where  $B(t)$  denotes the consistency of  $B$  cells,  $K_1$  and  $K_2$  represent the helper and suppressor genes,  $t$  denotes the  $t^{\text{th}}$  generation antigen consistency,  $d$  denotes the time delay of the immune response. Thus,  $\Delta B$  indicates the change in  $B$  cell consistency determined by Equation (6) [20].

$$\Delta B(t-d) = B(t-d) - B(t-d-1) \quad (6)$$

The immunological feedback loop has a dual purpose: it reacts quickly to foreign substances while maintaining immune system balance. However, antibodies are also ordered and

controlled since many may harm the body.

As a result, the deviation in a dynamic regulatory control system compatible with the immune system's goal [20] reduced to preserve system integrity. The amount of antigen  $\lambda(t)$  in Equation (5) represents the error  $e(t)$  controller's input will be the total incentive that the  $B$  cells accept.

$$e(t) = T - V_d \quad (7)$$

where  $V_d$  is desired input. Then the immune scheme system is defined as follows:

$$u_{im}(t) = K_1 \{1 - \eta_0 f[\Delta u(t - d)]\} e(t) \quad (8)$$

where  $K_1$  stands for the immune scheme gain indicated by the gene  $\eta_0 = K_2/K_1$ . The response speed is controlled by  $K_1$ , the stabilization effect is controlled by  $\eta_0$  and  $f[\cdot]$  denotes a nonlinear function. This function was selected because  $T$  cells regulate the action-function of antibodies in the immune response, which is affected by antigen consistency. The following is the definition of the function  $f[\cdot]$ :

$$f(x_{im}) = 1.0 - \exp\left(\frac{-x_{im}^2}{\alpha}\right), \quad \alpha > 0 \quad (9)$$

where  $\alpha$  parameter changes the function shape, the value of  $\alpha$  determines the active region of  $x_{im}$ . The output of the immune scheme is described as:

$$u_{im}(t) = K_1 \left\{ 1 - \eta_0 \left( 1.0 - \exp\left(\frac{-x_{im}^2}{\alpha}\right) \right) \right\} e(t) \quad (10 a)$$

$$u_{im}(t) = K_I e(t) \quad (10 b)$$

where  $K_I = 1 - \eta_0 \left( 1.0 - \exp\left(\frac{-x_{im}^2}{\alpha}\right) \right)$ . The immune scheme can consider as a nonlinear control gain.

#### IV. ADAPTIVE ROBUST IMMUNE POLE PLACEMENT CONTROL STRUCTURES

An Adaptive Robust Immune Pole Placement (ARIPP) controller is suggested to tracks the number of viruses given to patients in this article. ARIPP parameters tuned using The Improve Crow Search Algorithm (ICSA). The subject  $S_3$  studied utilizing pole placement and ARIPP with distinct structures. The interaction between oncolytic virus and cancer cells Equation (1) linearizes about the endemic equilibrium point  $Eqv = (S_{ss}, V_{ss}, I_{ss}; 0)$  using MATLAB function (*fsolve*) when  $U_v(t) = 0$ , and all states values differ from zero according to work in [14].

The state-space representation of the system after linearization described in the following equation:

$$\dot{X} = Ax + Bu \quad (11)$$

$$Y = Cx \quad (12)$$

$$U_v(t) = -kx \quad (13)$$

where  $X$  denotes the state vector,  $U_v$  referred to the control signal, and  $Y$  is the output ( $T$ ), then the system is written as a matrix as follows:

$$\begin{bmatrix} \dot{S} \\ \dot{I} \\ \dot{V} \end{bmatrix} = \begin{bmatrix} -r + r \ln\left(\frac{L}{S}\right) - \beta \frac{IV}{(I+S)^2} & \beta \frac{VS}{(I+S)^2} & -\beta \frac{S}{I+S} \\ \beta \frac{IV}{(I+S)^2} & -\beta \frac{IV}{(I+S)^2} - d_I & \beta \frac{S}{I+S} \\ 0 & \alpha d_I & -d_V \end{bmatrix} \begin{bmatrix} S \\ I \\ V \end{bmatrix} + \begin{bmatrix} 0 \\ 0 \\ 1 \end{bmatrix} U_v \quad (14)$$

$$Y = [1 \ 1 \ 0] \begin{bmatrix} S \\ I \\ V \end{bmatrix} \quad (15)$$

The matrix  $A$  will differ based on the equilibrium point chosen, but the matrices  $B$  and  $C$  will remain the same [14]. Since the system containing three states, it requires three gains:

$$k = -[k_1 \ k_2 \ k_3] \quad (16)$$

After determining the designed desired pole, the function (*place*) is used to get the state feedback gains. Since the pole placement control applied to a linear approach to extract the value of state feedback gains, therefore when these values used with the non-linear system, the controller performance is less efficiently when designed for the nonlinear system due to the loss of part of the nonlinear system properties by the linearization process. Furthermore, pole placement is not robust against noise and error induced by nonlinear disruption. Therefore, the immune scheme adds as an additional controller to change the pole placement gains according to error to solve this problem. Hence, the gain becomes adaptive values changing with system error change. The additional immune scheme connected serially with pole placement controller gains in different formats. The structure of varying controllers describes in the following subsection.

##### A. ARIPP STRUCTURE I

Fig. 1 shows a block diagram of this arrangement, in which the immune scheme gain multiplied by the pole placement controller's feedforward gain. Thus, the error signal  $e(t)$  serves as the input for the immune scheme.

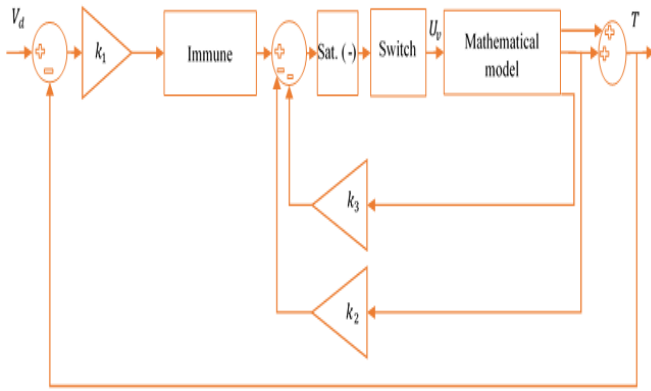


Figure 1: Block diagram of the APIPP structure I.

The first pole placement gain ( $k_1$ ) multiplied by the immune gain Equation (10 b) ( $K_I$ ), then for this structure, the controlling law is:

$$u_{to1}(t) = \text{sat}([1 - k_2 - k_3] \begin{bmatrix} u_{im1}(t) \\ 1 \\ 1 \end{bmatrix}) \quad (17)$$

$$u_{im1}(t) = K_I \times e_k(t) \quad (18)$$

where  $e_k(t) = k_1 \times e(t)$ , the  $\text{sat}(\cdot)$  is the saturation function limit upper and lower limit of control output and prevents the output from being negative because viruses can't be removed after they've been injected.  $k_i$  is state feedback gains where  $i = 1, 2, 3$  and  $K_I$  is immune scheme gain. The  $u_{to1}(t)$  signal then enters to be one of the switch inputs, and the other input is a signal built by the signal builder, which is the condition that works to pass the signal in specific periods and prevents it at different periods to simulate the injection process, so the final control signal be:

$$U_v(t) = \delta u_{to1}(t_1) + \delta u_{to1}(t_2) + \delta u_{to1}(t_i) + \dots + \delta u_{to1}(t_m) \quad (19)$$

where  $\delta$  max amplitude of control signal  $i$  day of injection and  $m$  is the period of treatment.

### B. ARIPP STRUCTURE II

Fig. 2 shows a block diagram of this arrangement, in which the immune scheme gain multiplied by each gain of the pole placement controller and sum with original gains.

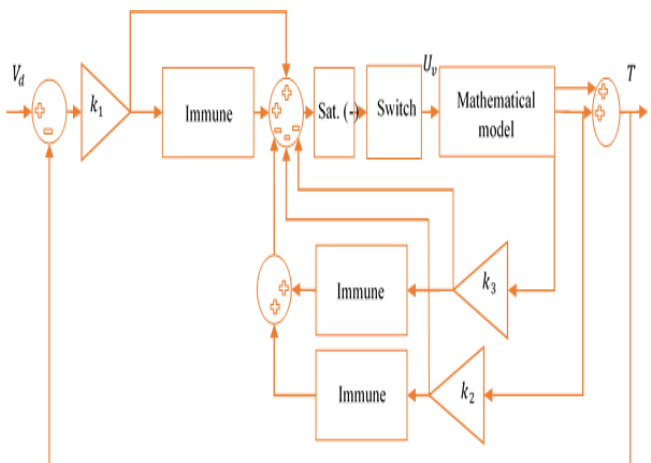


Figure 2: Block diagram of the APIPP structure II.

The controlling law for this structure:

$$u_{to2}(t) = \text{sat} \left( [-k_1 - k_2 - k_3] + \begin{bmatrix} u_{im1}(t) \\ u_{imj}(t) \\ u_{imn}(t) \end{bmatrix} \right) \quad (20)$$

$$u_{imj}(t) = K_I \times (k_j \times e(t)) \quad (21)$$

where  $j = 1, 2, \dots, n$ ,  $n$  system dimension. The  $u_{to2}(t)$  signal then enters to be one of the switch inputs, and the other input is a signal built by the signal builder, which is the condition that works to pass the signal in specific periods and prevents it at different periods to simulate the injection process, so the final output be same as Equation (19):

$$U_v(t) = \delta u_{to2}(t_1) + \delta u_{to2}(t_2) + \delta u_{to2}(t_i) + \dots + \delta u_{to2}(t_m) \quad (22)$$

where  $\delta$  max amplitude of control signal  $i$  day of injection and  $m$  is the period of treatment

### C. ARIPP STRUCTURE III

Block diagram of this structure is shown in Fig. 3. The pole placement control signal multiply by immune gain.

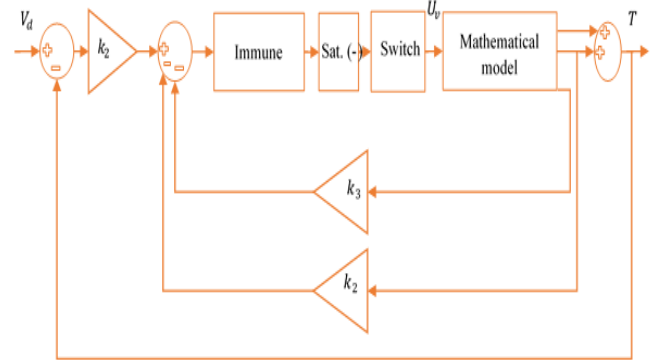


Figure 3: Block diagram of the APIPP structure III.

The controlling law is:

$$u_{to3}(t) = \text{sat}(K_I \times [-k_1 - k_2 - k_3]) \quad (23)$$

The exact process in previous structures have flowed to construct the final control output:

$$U_v(t) = \delta u_{to3}(t_1) + \delta u_{to3}(t_2) + \delta u_{to3}(t_i) + \dots + \delta u_{to3}(t_m) \quad (24)$$

where  $\delta$  max amplitude of control signal  $i$  day of injection and  $m$  is the period of treatment

### V. IMPROVE CROW SEARCH ALGORITHM (ICSA)

The crow search algorithm (CSA) behaviour inspires by crows' clever food-hiding. It extensively utilized to handle various optimization problems, and it's outperformed several contemporary optimization algorithms in the literature [21]. In the original CSA, "the constraints are directly handled. It means that each solution that cannot satisfy the conditions altogether will be considered as

infeasible and abandoned" [8]. The rejection of impossible solutions may be severe flaws to the design space problems and dominated by constraints. Hence, creating a possible design for such problems may take an enormous number of successive trials [8]. To maintain a good balance between exploration and exploitation, the following additions propose: First, multiply the current position equation by the inertia factor  $\sigma$  [22].  $\sigma$ 's value would decline over time. The linear regression of factor  $\sigma$  is determined as follows in general [23]:

$$\sigma(t) = \sigma_{max} - (\sigma_{max} - \sigma_{min}) \times \frac{iter}{Maxiter} \quad (25)$$

where  $iter$  represents the number of repetitions,  $\sigma_{max}$  and  $\sigma_{min}$  are the upper and lower limits of  $\sigma$  factor and

$Maxiter$  maximum number of iterations. Equations of position update become:

$$P_i^{t+1} = \begin{cases} \sigma \times P_i^t + r_1 \times FL_i^t \times (M_j^t - P_i^t), & \text{if } r_2 \geq AP_i^t \\ \text{random position,} & \text{otherwise} \end{cases} \quad (26)$$

where  $P_i^t$  Position matrix representing the position of each crow  $i$  at iteration  $t$ ,  $M_j^t$  Memory matrix where hiding places positions are stored,  $r_1$  and  $r_2$  random numbers with a uniform distribution between 0 and 1,  $FL$  flight length and  $AP$  awareness probability. Secondly, adding a treatment to the new position is produced before determining. the flow chart below shows the implementation of ICSPA:

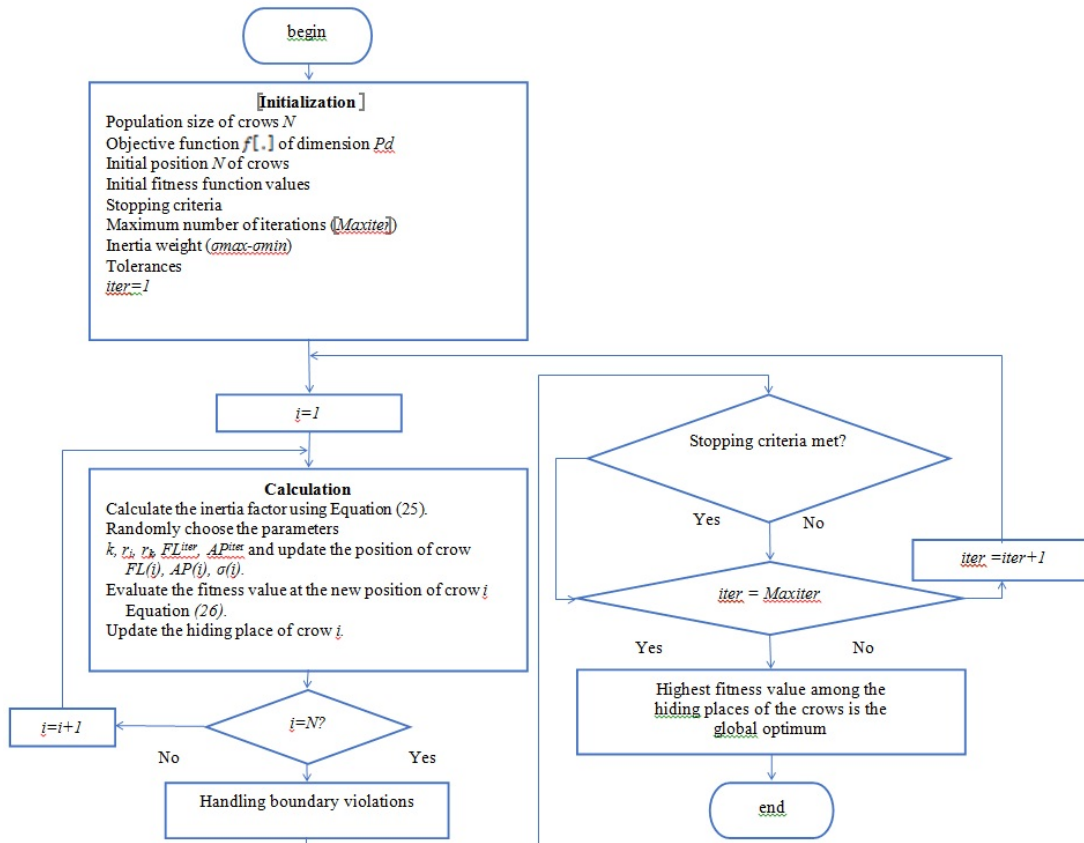


Figure 4: ICSPA flow chart.

## VI SIMULATION RESULTS AND ANALYSIS

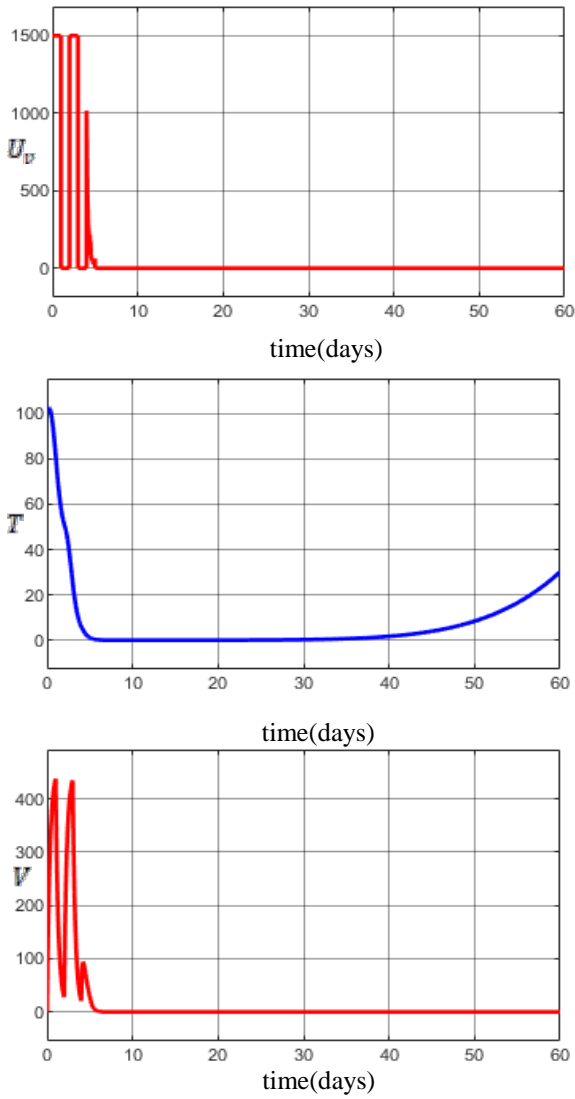
In this part, the suggested ARIPP controller with the structures (I, II, and III) based on the ICSPA for controlling the interaction between tumor and virus models was evaluated using MATLAB 2019. The treatment objective is to decrease and maintain the total number of tumor cells below 50 cells within 60 days. Fig. 5 shows the model reaction to the subjects  $S_3$  using the pole placement controller based ICSPA. The findings indicate that after a viral injection is completed, the total tumor volume ( $T$ ) maximum is reached. The control parameters obtained using ( $place$ ) instruction for  $S_3$  are listed in Table II when  $\xi = 1, \omega_n = 4 \text{ rad/sec}$ .

Table II: Parameters for pole placement controller based ICSPA.

$k1$	$k2$	$k3$
-175.9406	-21.7704	6.4777

In Fig. 5, The top figure illustrates the viral injections over 60 days. The middle figure illustrates the total number of tumor cells. The bottom figure shows the viral loads in vivo. Treatment fails to maintain the tumor within the therapeutic zone, where the tumor begins to regress after an initial rise.

This controller has various effects on different subjects. Performance of proposed controllers' structures based on ICSPA for parameters optimization follows the treatment protocol of injection a high dose at days 0, 2, 4 because "Studies of a broad array of human solid tumor types revealed that cell cycle progression lasts two days, on average" [6], describes in the following subsection. The parameters used in the optimization algorithm for all structures listed in Table III.



**Figure 5:** Treatment of subject  $S_3$  with pole placement controller.

**Table III:** ICOSA algorithm parameters.

Parameters	Value
Population size ( $N$ )	25
Max iteration (Maxiter)	50
Problem dimension ( $Pd$ )	3, 5, 9
Awareness probability ( $AP$ )	1.2
Flight length ( $FL$ )	0.3
Inertia weight ( $\sigma_{max}-\sigma_{min}$ )	(0.9 – 0.4)

#### A. ARIPP STRUCTURE I RESPONSE

The state feedback gains that get using (*place*) function and the immune scheme parameter that get its initial value from literature are used as an initial value for ICOSA and optimized by multiplying it's in random values between (1 - 5) The state feedback gains and (1 - 2, 0.01 - 1) for the immune scheme. The optimal parameters list in Table IV, and the response shown in Fig. 6 below.

**Table IV:** Optimal parameters for ARIPP controller structure I based ICOSA

$k_1$	$k_2$	$k_3$	$K_I$	$\eta_0$
-229.8136	-21.7704	6.4777	3.8160	0.6066

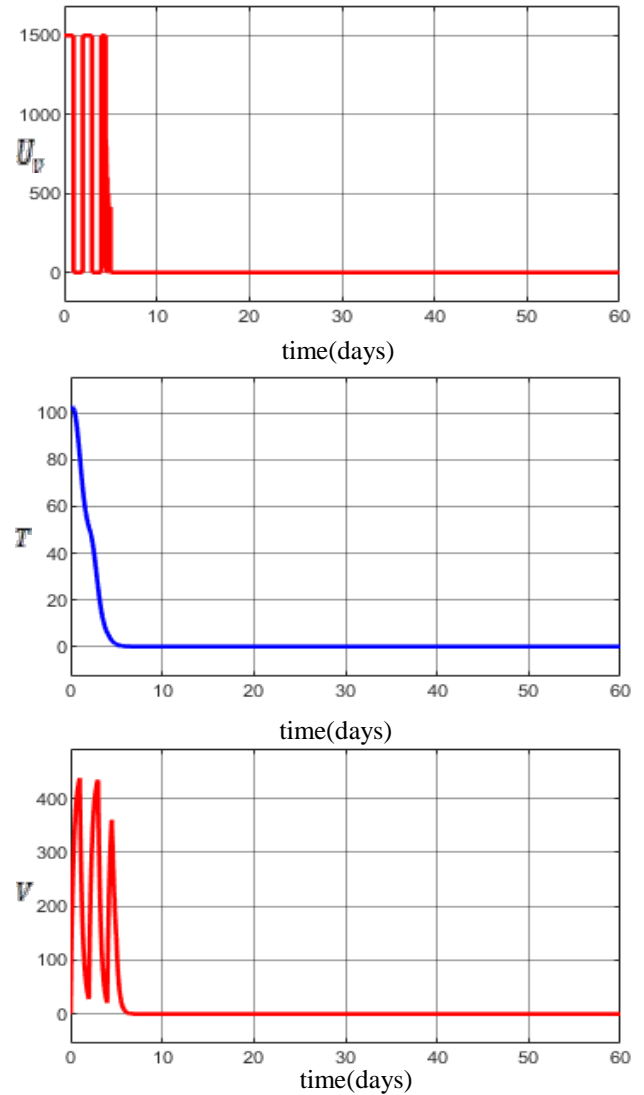


**Figure 6:** Simulation result of  $S_3$  using ARIPP I structure based ICOSA.

#### B. ARIPP STRUCTURE II RESPONSE

The same procedure in structure I flow in structure II. The optimal parameters list in Table V, and the response is shown in Fig. 7 below.

**Table V:** Optimal parameters for ARIPP controller structure II based ICOSA

$k_1$	$k_2$	$k_3$	$K_{I1}$	$K_{I2}$
-798.4184	-67.8845	6.6202	4.4376	4.8169
$K_{I3}$	$\eta_{01}$	$\eta_{02}$	$\eta_{03}$	$K_{I3}$
3.9644	0.4156	0.0230	0.3062	3.9644

#### C. ARIPP STRUCTURE III RESPONSE

The procedure flowed in structure I and structure II also applied in structure III. The optimal parameters list in Table VI, and the response is shown in Fig. 8.

**Table VI:** Optimal parameters for ARIPP controller III structure based ICSEA

$k_1$	$k_2$	$k_3$	$K_I$	$\eta_0$
-713.2984	-63.8613	6.4777	5.7835	0.6066

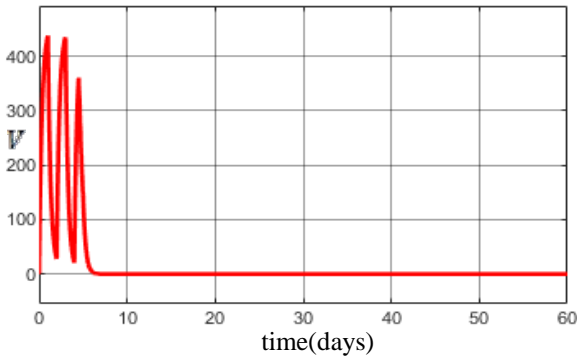
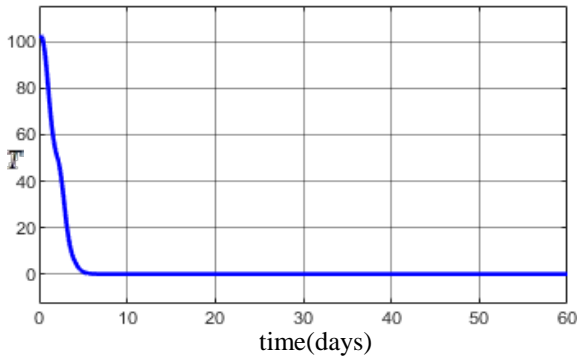
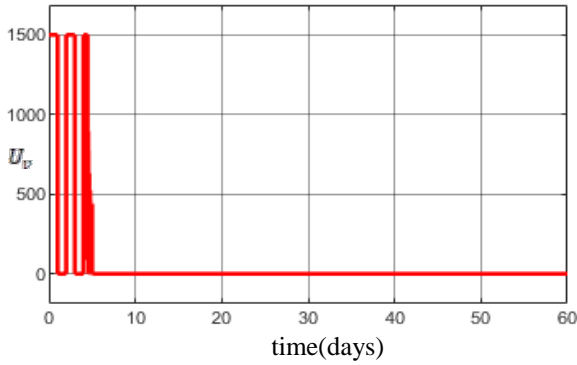


**Figure 7:** Simulation result of  $S_3$  using ARIPP II structure based ICSEA.

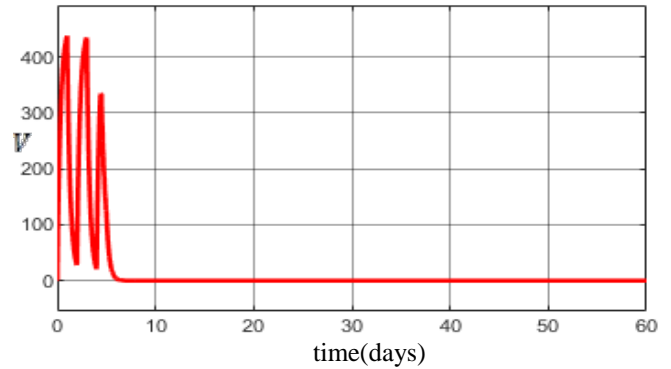
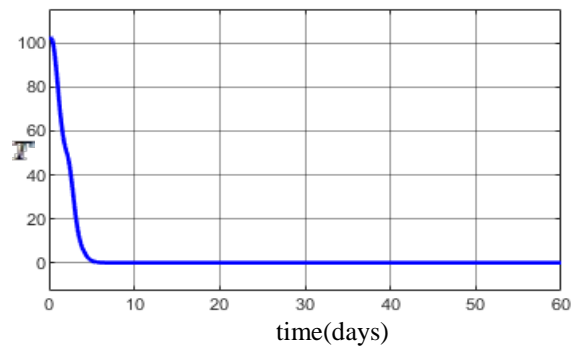
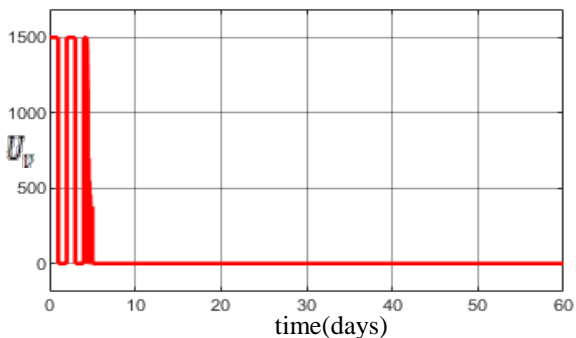


**Figure 8:** Simulation result of  $S_3$  using ARIPP structure III based ICSEA.

In Fig. 6, 7, 8, the top figure illustrates the total number of tumor cells for 60 days. The middle figure shows the viral loads in vivo. The bottom figure illustrates the viral injections within three days.

In all the ARIPP control structures, there are no rebounds of the tumor after the end of the treatment. The internal immune scheme works to keep the tumor with a therapeutic zone, i.e., less than or equal to 50 total tumours cells, and reduce the amount of injections over time as showing in Figure 6, 7, 8 (top figures). The feedback mechanism in the immune scheme increases the number of injections due to an increase in  $\eta_0$  the larger ratio indicates the increase of  $T_h$  cells, whose increase leads the body to form more antibodies to protect itself. As a result, the control signal is lower in treatment with the ARIPP controller than in pole placement during the last hours of treatment and decreases gradually, as shown in Fig. 6, 7, 8 (middle figures). Nevertheless, the virus load tends to be identical in the pole placement and ARIPP, except for the last injection where be higher to eliminate rebounded tumor.

The results suggest applying ARIPP control in oncolytic virotherapy has benefited by delivering an adequate amount of treatment to accomplish therapeutic goals, as all proposed structures of ARIPP controllers performs this task and give the excellent result the ARIPP stricter I superior performance II and III structures by 3.2707%, 3.5452% respectively, where the performance index used is Integral Time Absolute Error (ITAE).

Furthermore, the controller test against dynamic uncertainty as in [14], where the logarithm term in the interaction between oncolytic virus and cancer cells Equation (1) replaced with exponential  $rS(t)$ , the result shows the

robustness of the proposed controller against dynamic uncertainty. Response using the structure I shown in Figure 9 and optimal parameter listed in Table VII.

**Table VII:** Optimal parameters for ARIPP controller structure I based ICOSA

$k_1$	$k_2$	$k_3$	$K_I$	$\eta_0$
-235.7252	-36.4458	6.4777	4.54104	0.3222

## VII CONCLUSION

An artificially adjusted ARIPP controller with different structures (I, II, and III) has been proposed to manage the amount of viral load injections given to limit tumor cell

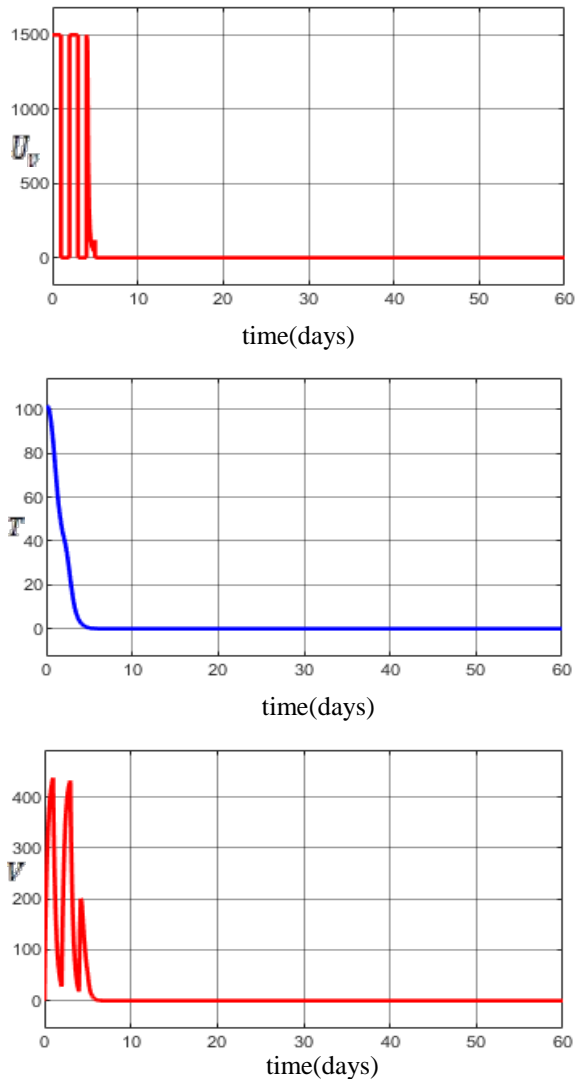


**Figure 9:** Simulation result of  $S_3$  using ARIPP I structure based ICOSA.

proliferation. In addition, the mathematical model of cancer cell-oncolytic virus interaction has been taken into consideration. ICOSA has been used to get best set of parameters for the suggested controllers. According to the simulation findings, the ARIPP structure I perform better than the other structures. Finally, the immune scheme improves the control efficiency, makes the controller more robust against dynamic uncertainty, and prevents the tumours from growing after therapy time frame complete. This will

enable cancer suppression later via surgery, allowing patients to live as long as possible and reduce the number of injections. Toxicity not considered as an issue because when using an oncolytic adenovirus coated with a biocompatible polymer, such as polyethylene glycol (PEG) case toxicity can be neglected.

As a next step, need to do further mathematical and experimental research to understand better the connection between toxicity, the number of viral injections, and the number of virally infected cells in vivo. Though these results may assist create new viral treatments and tumor management methods, they will also help speed up new medicines and tactics to maximize tumor regression with minimum adverse effects.

## REFERENCES

- [1] Cancer Research UK, "Worldwide cancer statistics | Cancer Research UK," Cancer Research UK. pp. 1–5, 2016. Accessed: Apr. 26, 2021. [Online]. Available: <https://www.cancerresearchuk.org/health-professional/cancer-statistics/worldwide-cancer>
- [2] NIH, "Cancer Statistics - National Cancer Institute," NIH, 2016. <https://www.cancer.gov/about-cancer/understanding/statistics> (accessed Apr. 26, 2021).
- [3] A. L. JENNER, "Applications of mathematical modelling in oncolytic virotherapy and immunotherapy," Bulletin of the Australian Mathematical Society, vol. 101, no. 3, pp. 522–524, 2020.
- [4] [4] R. Padmanabhan, N. Meskin, and A.-E. al Moustafa, Mathematical Models of Cancer and Different Therapies: Unified Framework. Springer Nature, 2021.
- [5] A. K. Arum, D. Handayani, and R. Saragih, "Robust control design for virotherapy model using successive method," in Journal of Physics: Conference Series, 2019, vol. 1245, no. 1, p. 12054.
- [6] J. J. Crivelli, J. Földes, P. S. Kim, and J. R. Wares, "A mathematical model for cell cycle-specific cancer virotherapy," Journal of biological dynamics, vol. 6, no. sup1, pp. 104–120, 2012.
- [7] A. Kaur, R. Kaur, and S. Sondhi, "CSA based PID controller design technique for optimizing various integral errors," in 2020 10th International Conference on Cloud Computing, Data Science & Engineering (Confluence), 2020, pp. 55–62.
- [8] A. Askarzadeh, "A novel metaheuristic method for solving constrained engineering optimization problems: crow search algorithm," Computers & Structures, vol. 169, pp. 1–12, 2016.
- [9] K. Takahashi and T. Yamada, "Application of an immune feedback mechanism to control systems," JSME International Journal Series C Mechanical Systems, Machine Elements and Manufacturing, vol. 41, no. 2, pp. 184–191, 1998.
- [10] Y. Ding, L. Chen, and K. Hao, Bio-Inspired Collaborative Intelligent Control and Optimization. Springer, 2018.
- [11] J. Sun et al., "Optimal control model of tumor treatment with oncolytic virus and MEK inhibitor," BioMed research international, vol. 2016, no. 3–4, pp. 3763–3775, 2016.
- [12] J. Malinzi, R. Ouifki, A. Eladdadi, D. F. M. Torres, and K. A. White, "Enhancement of chemotherapy using oncolytic virotherapy: mathematical and optimal control analysis," arXiv preprint arXiv:1807.04329, 2018.
- [13] A. K. Arum, R. Saragih, and D. Handayani, "Bilinear robust control design for virotherapy model," in 2019 19th International Conference on Control, Automation and Systems (ICCAS), 2019, pp. 82–86.
- [14] A. J. N. Anelone, M. F. Villa-Tamayo, and P. S. Rivadeneira, "Oncolytic virus therapy benefits from control theory," Royal Society open science, vol. 7, no. 7, p. 200473, 2020.
- [15] M. F. Villa-Tamayo, A. J. N. Anelone, and P. S. Rivadeneira, "Tumor Reduction Using Oncolytic Viruses Under an Impulsive Nonlinear Estimation and Predictive Control Scheme," IEEE Control Systems Letters, vol. 5, no. 5, pp. 1705–1710, 2020.
- [16] P.-H. Kim et al., "Active targeting and safety profile of PEG-modified adenovirus conjugated with herceptin," Biomaterials, vol. 32, no. 9, pp. 2314–2326, 2011.
- [17] A. L. Jenner, C.-O. Yun, P. S. Kim, and A. C. F. Coster, "Mathematical modelling of the interaction between cancer cells and an oncolytic virus: insights into the effects of treatment protocols,"

- Bulletin of mathematical biology, vol. 80, no. 6, pp. 1615–1629, 2018.
- [18] A. L. Jenner, P. S. Kim, and F. Frascoli, “Oncolytic virotherapy for tumours following a Gompertz growth law,” *Journal of theoretical biology*, vol. 480, pp. 129–140, 2019.
- [19] X. Liu, X. Chen, X. Zheng, S. Li, and Z. Wang, “Development of a GA-fuzzy-immune PID controller with incomplete derivation for robot dexterous hand,” *The Scientific World Journal*, vol. 2014, 2014.
- [20] B. Rochdi, “Design and application of fuzzy immune PID control based on genetic optimization,” in *International Workshop on Advanced Control IWAC*, 2014, pp. 10–14.
- [21] Y. Meraihi, A. B. Gabis, A. Ramdane-Cherif, and D. Acheli, “A comprehensive survey of Crow Search Algorithm and its applications,” *Artificial Intelligence Review*, pp. 1–48, 2020.
- [22] Y. Shi and R. Eberhart, “A modified particle swarm optimizer,” in *1998 IEEE international conference on evolutionary computation proceedings. IEEE world congress on computational intelligence (Cat. No. 98TH8360)*, 1998, pp. 69–73.
- [23] J. Sun, W. Fang, V. Palade, X. Wu, and W. Xu, “Quantum-behaved particle swarm optimization with Gaussian distributed local attractor point,” *Applied Mathematics and Computation*, vol. 218, no. 7, pp. 3763–3775, 2011.